Caving 2026 – A van As, D Cumming-Potvin & J Wesseloo (eds)

doi:10.36487/ACG_repo/2645_93

Quantifying excavation response to accurately inform numerical modelling analysis at Oyu Tolgoi

Karta Simanjuntak [a,*], Glenn Sharrock [c], Lawrence Rwodzi [a], Josef Ekkerd [a], Juma Mgumbwa [b], Ferric Mardiansyah [b]

[a] *Oyu Tolgoi, Rio Tinto, Australia*

[b] *Oyu Tolgoi, Rio Tinto, Mongolia*

[c] *ITASCA, Australia*

Abstract

The Panel 0 footprint at Oyu Tolgoi has been successfully established in a structurally complex rock mass of variable strength at a depth of 1,300 m. To monitor the rock mass response and the excavation stability, Panel 0 was well instrumented with multipoint borehole extensometers, convergence pins, borehole monitoring, convergence scanning and damage mapping. Thus, during undercutting to surface breakthrough, extensive data related to footprint stability performance were collected on extraction, undercut and apex levels. This data was analysed using conventional data analysis and numerical methods to delineate ground reactions and ground behaviour. Assessments indicated ground behaviour is influenced by several parameters including (a) geotechnical properties, (b) faults and defects, and (c) mining-induced stress. Mining-induced stress is influenced by local excavation geometry, cave volume, cave shape and distance from the cave. The objective of this paper is to share the framework developed to understand ground behaviour through analysis of the monitoring data and numerical modelling.

Keywords: *Oyu Tolgoi, block cave, monitoring data, stability, caveability, convergence, numerical model, FLAC3D, bonded block modelling, calibration*

1 Introduction

The objective of this paper is to share the developed framework of the geotechnical stability calibration of Panel 0 driven by the actual data Figure 1 describes the general process which starts with data collection, including understanding of the instrumentation, data definition and limitations, then data QA/QC, ground responses driving factor analysis, and numerical modelling calibration and forecasting.

* Corresponding author. Email address: Karta.Simanjuntak@riotinto.com

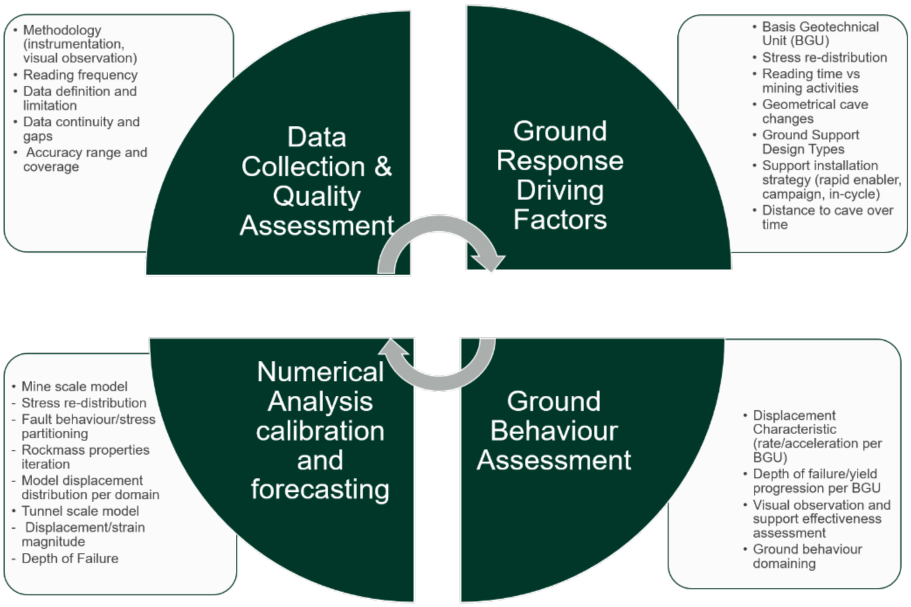

Figure 1 The process flow of geotechnical data collection and assessment to inform numerical modelling analysis based on the observational method

1.1 Geology and geotechnical conditions

The Hugo North deposit comprises porphyry-style mineralisation and associated alteration assemblages related to quartz monzodiorite (QMD) intrusions emplaced beneath a deformed sequence of Upper Devonian to Lower Carboniferous sedimentary and volcanic rocks. The deposit forms an elongated orebody oriented approximately north-northeast–south-southwest, extending over 3 km in strike length (Figure 2a). QMD, augite basalt (VA) and ignimbrite (IGN) constitute the principal mineralised lithologies within the orebody. Biotite granodiorite (BiGd) represents a late- to post-mineralisation intrusive phase, forming a dyke system along the western and central portions of the deposit, with more restricted dykes and sills present elsewhere.

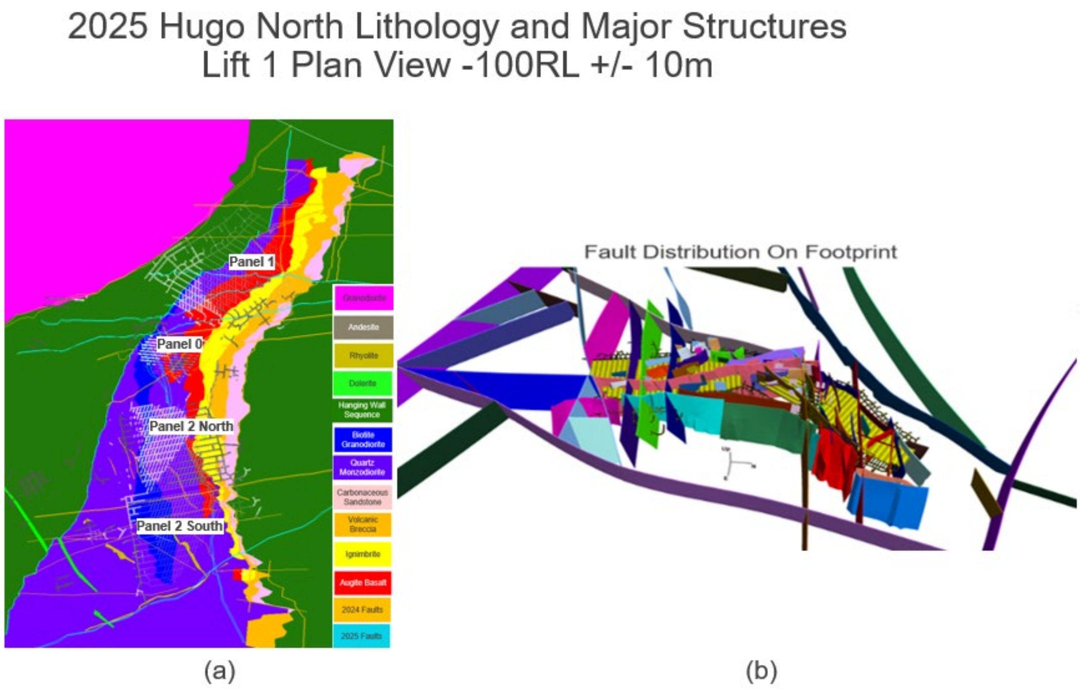

Figure 2 (a) Hugo North Lift-1 lithology model at RL-100; (b) Major fault distribution on Lift 1

Based on the in situ rock mass rating (RMR) (Laubscher 1990) values, the Panel 0 footprint is generally characterised by fair to good rock mass quality However, it is a highly fault-dominated environment, as shown in Figure2b. Panel 0 lithology is shown in Figure 3a, and major faults or mine scale faults and minor faults are situated across the entire footprint, mapped as mostly having poor ground conditions and low-strength rock mass (Figure 3).

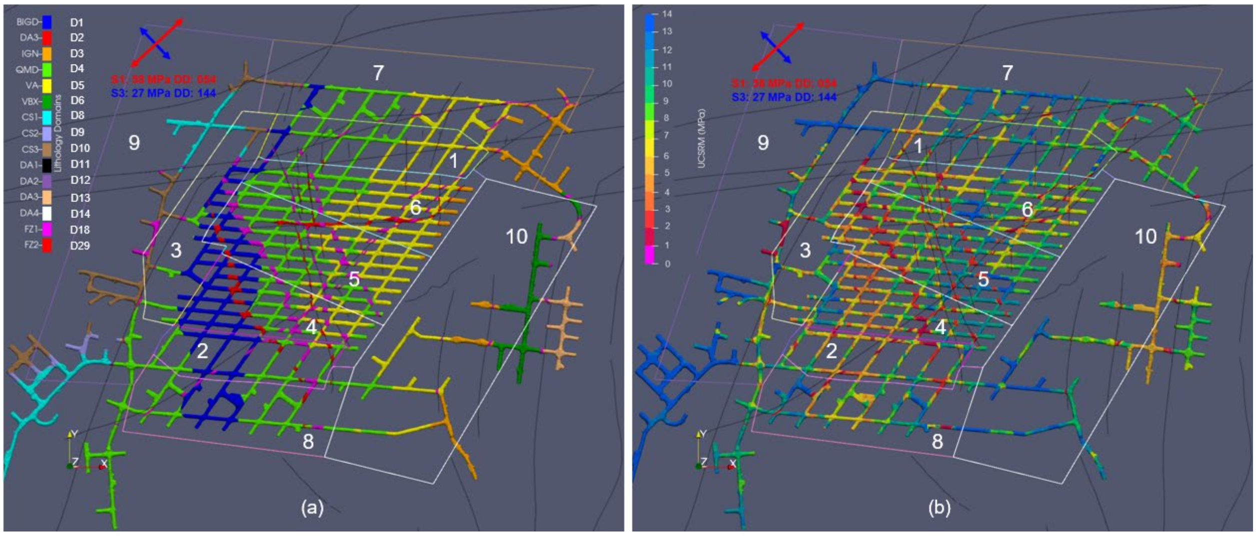

Figure 3 Panel 0 footprint: (a) Lithology and primary calibration domains (D1 to D29); (b) Rock mass uniaxial compressive strength

The intact rock strength within the Panel 0 footprint generally ranges between 65 and 80 MPa, with representative values of Geological Stability Index (GSI) of 60 and Laubscher's RMR (RMRL90) of approximately 45. At a depth of approximately 1,300 m below surface, the major, intermediate and minor principal stresses are estimated to be 58, 35 and 27 MPa, respectively, with both the major and minor principal stresses dipping sub-horizontally (Bayar et al. 2024). Under these rock mass and in situ stress conditions, excavation behaviour within the footprint is expected to be dominated by stress-induced failure mechanisms characterised primarily by rock bulking around tunnel walls and squeezing ground conditions, particularly in areas influenced by weaker fault-related material.

1.2 Block cave design principles at Panel 0

The Panel 0 block size is approximately 300 × 250 m. As shown in Figures 3a and b, the major principal stress direction is 54^{o} azimuth. The undercut was initiated from the southwest corner of Panel 0 block and advances towards the northeast corner with a maximum of 10 m undercut lead-lag. The undercutting was completed in 2.5 years with an undercut advance rate of 10 to 15 m per month. A 4.9 m-wide × 4.5 m-high drive is the typical extraction level (EXL) drive dimension, with a 400 kPa estimate ground support pressure system applied.

2 Geotechnical monitoring data collection

2.1 Data collection and methodology

Oyu Tolgoi Panel 0 is one of the most extensively instrumented block cave footprints (Ulziijargal 2024). multipoint borehole extensometers (MPBXs) and tape convergence pins were installed at each drawpoint pillar, or generally at approximately 20 m intervals across the footprint. Mobile and static lidar scanners are used to monitor tunnel profile deformation, producing point cloud-based displacement data. In addition, tunnel borehole camera inspections and visual damage mapping are conducted to assess tunnel deformation and ground support conditions. While this comprehensive monitoring system provides a robust dataset for ground response assessment, it also introduces significant data management challenges due to the high volume and variety of data collected. To address this, Oyu Tolgoi utilises the Foundry system to facilitate monitoring data management, integration and visualisation (Ulziijargal 2024). It is important to note that collected data from different instrumentation systems or observation methodologies are not straightforward comparable datasets. A clear understanding of the definition of the data and its limitations will later inform the data analysis and interpretation process. Table 1 below summarises the data collection methodology, data definitions and limitations used in Panel 0.

Table 1 Data collection methodology, data definitions and limitations

Notional accuracy	Methodology	Description	Definition and limitation	Reading frequency
0.1 mm	Multipoint borehole extensometer	Instrumentation	Point displacement versus depths Less sensitivity to tunnel skin movement Maximum reading is 243 mm Significant effort for replacement if damaged/ high interruption to data continuity	Network connected device/hourly
1 mm	Tape convergence pins	Instrumentation	A single point displacement of the tunnel skin movement A quick replacement process or a high data reading continuity	Weekly
20–30 mm	Mobile lidar scan	Instrumentation	Point cloud tunnel skin movement Footprint to mine scale coverage Lower accuracy of 20–30 mm Requiring clear access to the footprint/irregular data collection frequency	Monthly or clear access to the footprint
1.0 mm	Static lidar scan	Instrumentation	Point cloud tunnel skin movement Specific local coverage Low data continuity	Specific period in the concern area only/by cases
Rating system	Tunnel borehole camera	Visual observation	Visual observation of the ground condition behind the wall through a borehole Subjective or observer-dependent data Used for tracking the depth of fracture estimate	Monthly to weekly
Rating system	Tunnel damage mapping	Visual observation	Visual observation of tunnel skin condition Subjective or observer-dependent data Capture tunnel behaviour/failure mechanism	Monthly to weekly

2.2 Data processing and review

A systematic data quality review and cleaning process is required prior to data interpretation and its use in subsequent analyses such as numerical modelling. Given the large volume of monitoring data generated across the footprint, a relatively high proportion of invalid or non-representative data is expected. Key parameters reviewed to ensure data alignment and comparability across instruments and observation methods include the initial and final reading dates, measurements exceeding instrument capacity, irregular or non-physical trends, initial value offsets and extended periods of missing data. These data conditions are described in Figure 4.

Damage mapping provides additional important information about the extent and condition of damage to the surface support; these data proved extremely important. However, when used in isolation, this data does not provide a conclusive or definitive description of factors controlling rock mass deformation. To understand the rock damage and deformation mechanism, multiple methods are required to collect data on damage and deformation parameters.

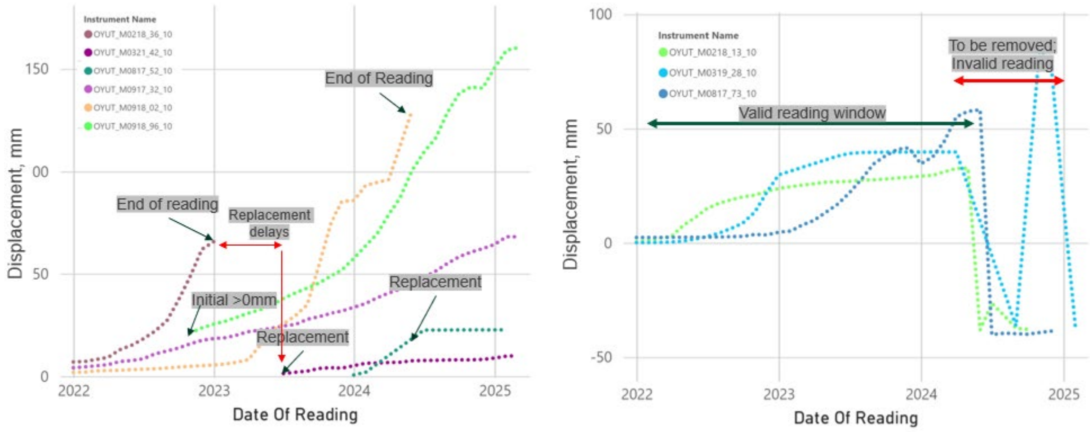

Figure 4 Example of data conditions to be addressed during data quality assessment

The reviewed and cleaned datasets are subsequently available for comparative plotting over time and for overlay with other instrumentation within the footprint. Care must be taken to ensure that comparisons are made only between instruments with equivalent reading windows.

2.3 Driving factors and data grouping

The primary drivers of ground response variability across the footprint are rock mass variability and stress redistribution associated with cave advance. While rock mass variability represents an inherent condition, stress redistribution is dynamic and largely controlled by mining activities including undercutting, draw control and associated cave growth, and lateral development. A data-grouping approach based on these two factors was therefore adopted. The primary objective of this approach is to minimise the influence of local-scale rock mass variability that is not fully captured by geological and geotechnical mapping.

Under similar stress-change conditions, for example within polygon Below_3 shown in Figure 5, different rock mass properties or geotechnical units within the same polygon exhibit varying ground responses. Conversely, the same rock mass properties can produce different responses when subjected to different stress-change environments across polygons. As illustrated in Figure 6, ground response data within the Below_3 polygon are predominantly influenced by cave abutment stress, whereas responses within polygons Below_2 and Below_1 are primarily driven by cave static loading, as these areas were passed by the undercut earlier and have since transitioned into a different stress regime. Understanding the dominant drivers controlling each recorded ground response is therefore essential to support the interpretation of failure mechanisms and to effectively inform numerical model calibration and forecasting.

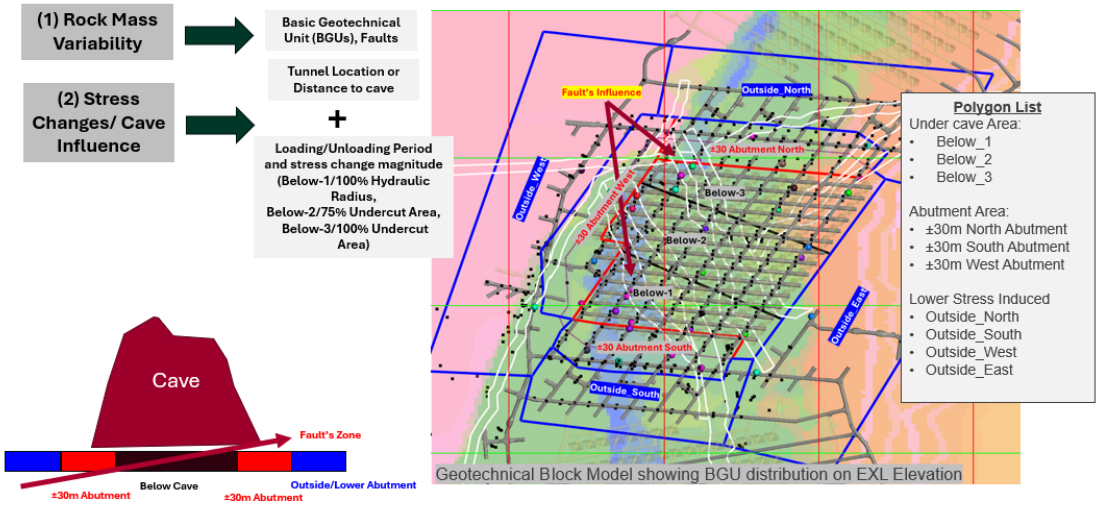

Figure 5 Panel 0 data grouping methodology based on rock mass and stress change variability

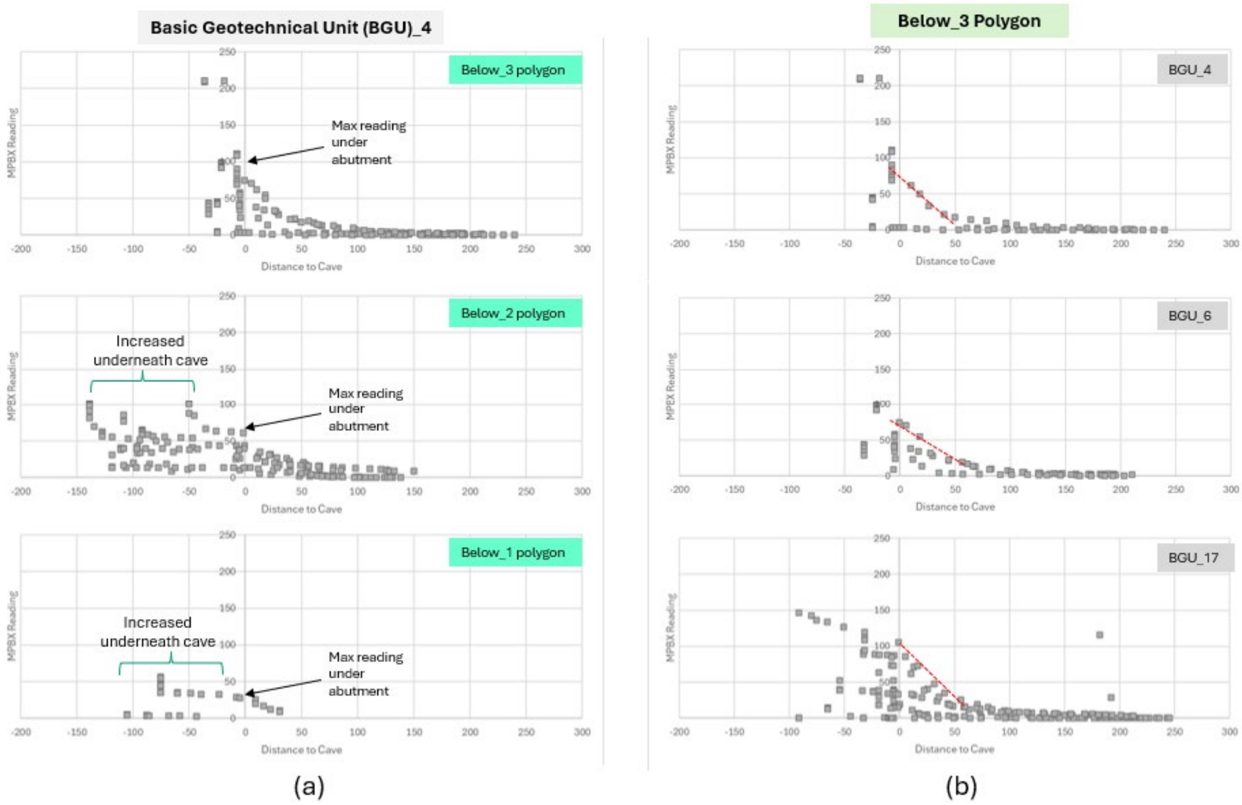

Figure 6 (a) An example of ground response variance at different stress change condition but within similar rock properties; (b) An example of ground response variance at different rock properties but within similar stress change conditions

Mine scale numerical analysis concern is typically the treatment of observational and numerical data for heterogeneous systems. Because the arrangement of defects influencing individual instruments is unknown, numerical analysis instead considers ground behaviour within statistical partitions or bins rather than for individual instruments. A bonded block model is used to assess local ground responses in a selected area.

3 Monitoring data interpretation

3.1 Wall and back movement correlation

Stress changes are defined as the redistribution of stresses around the cave resulting from geometric changes to the size and shape of the void generated by undercut advance and cave draw, ultimately facilitating vertical cave propagation. Compressional stress conditions within the abutment zone, stress rotation towards the cave front and reduced confinement beneath the cave, accompanied by a gradual increase in cave material static load, represent the primary stress regimes experienced by most EXL excavations. In Panel 0, the influence of these stress changes is captured by the observed ground response derived from the monitoring data.

During undercutting, pronounced wall movements were commonly observed within EXL abutment areas, driven by elevated vertical cave-induced stresses developed near the advancing undercut front. Beneath the cave, ongoing drawpoint development and drawbell blasting complete the formation of major and minor pillars. In these zones, reduced confinement combined with increasing cave material static loading has resulted in enhanced pillar wall convergence, followed by progressive back movement. Wall convergence reflects a deepening of the tunnel depth of failure, effectively increasing the excavated span and consequently reducing the stability of the formed roof beam. This mechanism is described in Figure 7 using wall and back displacement data from Panel 0.

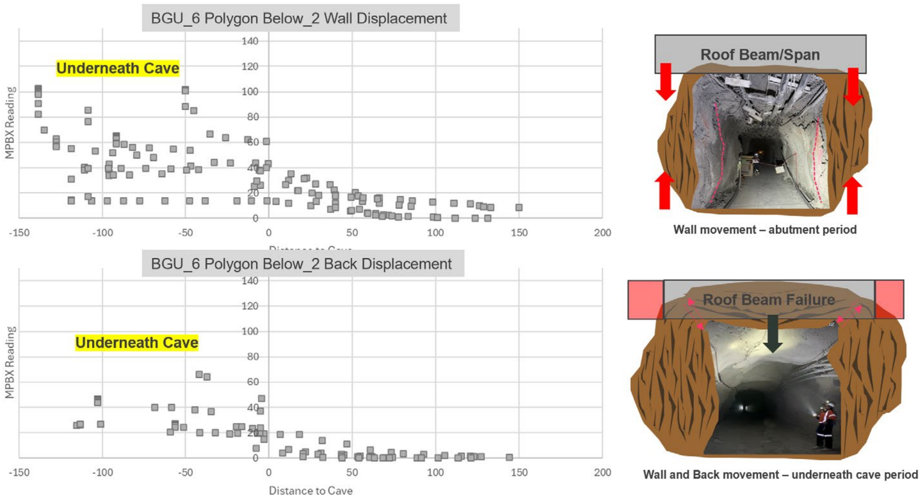

Figure 7 Back and wall displacement of basic geotechnical unit (BGU) 6 plotted against distance to cave

3.2 Depth of fracture and depth of yield

Depth of fracture (DoF) and its progressive deepening over time represent a key indicator for assessing excavation failure mechanisms. In Oyu Tolgoi Panel 0, several boreholes were drilled prior to undercut initiation to establish the initial DoF of the tunnels, which is predominantly associated with development blasting damage and tunnel baggage. Borehole camera data are grouped by geotechnical unit and stress change polygon, as described in previous sections, enabling interpretation of DoF development in the context of rock mass properties and evolving stress conditions. Figure 8a presents a summary of borehole camera observations across Panel 0 to date, indicating that the DoF generally ranges between 1.0 and 3.0 m. Notably, the DoF varies between geotechnical units and locations, reflecting differences in rock mass characteristics and stress environments. These observed variations are subsequently used to inform numerical model calibration.

Depth of yield (DoY), defined as the extent of plastic zone or non-recoverable deformation within the rock mass, is interpreted using MPBX data. The MPBX datasets are grouped using the same geotechnical unit and stress polygon framework applied to the DoF analysis. Figure 8b illustrates an example of MPBX displacement data plotted by anchor depth against cave development phases, representing the progression of DoY with time. Across Panel 0, the DoY is generally observed to range between 4.0 and 7.0 m. The development of both DoF and DoY is primarily stress-driven, with progressive deepening occurring during periods of elevated cave abutment stress and continuing under conditions of reduced confinement when the area is transitioned to beneath cave stress condition.

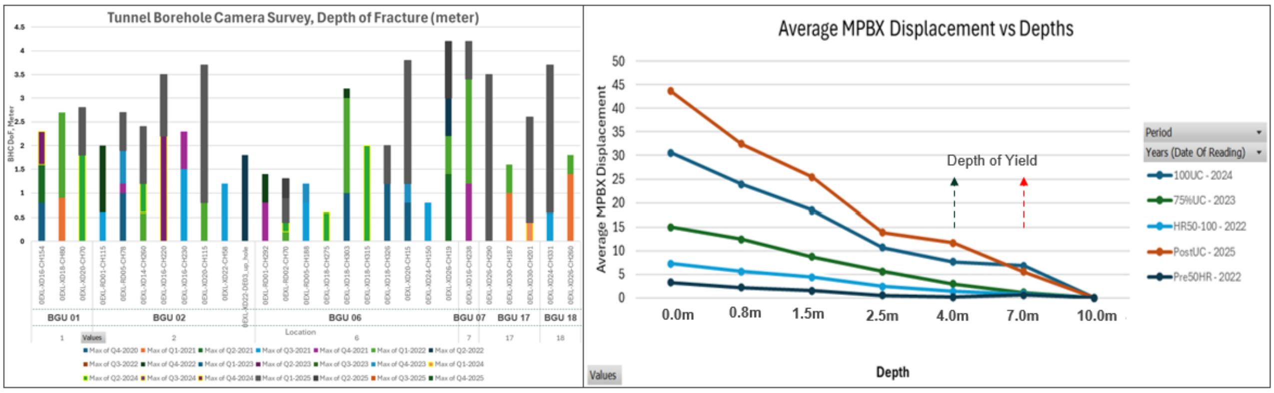

(a) (b)

Figure 8 (a) Depth of fracture in Panel 0 based on visual observation through a borehole camera; (b) An example of Depth of yield measurement based on multipoint borehole extensometers (MPBX) displacement plot

3.3 Tunnel damage mechanism

The dominant damage mechanism in Panel 0 was a stress-driven failure where rock spalling occurred behind the walls. This manifested with an observed rock bulking condition on the tunnel walls positioned in alignment with the loading direction and within the fair to good rock quality. With poorer rock mass quality, such as tunnels situated within fault material influence, a rapid convergence on walls and the back of the tunnel is monitored once the tunnel is under abutment stress. Further movement occurs once pillars are formed and cave material static load affects the tunnels under the cave area.

While the rock is under higher stress conditions in the abutment area, a rock mass quality degradation is expected due to a stress-driven failure occurring. This is indicated by the formation of new cracks or displacement at a joint or vein system within the tunnel yielded zone. Therefore, when the rock is transitioned to be under the cave stress regime, the rock mass quality is degraded to a lower class (or M32 from M23) as described in Figure 9 below. Subsequently, the rock mass failure mechanism is transitioned from stress-driven failure to a stress-assisted failure mechanism.

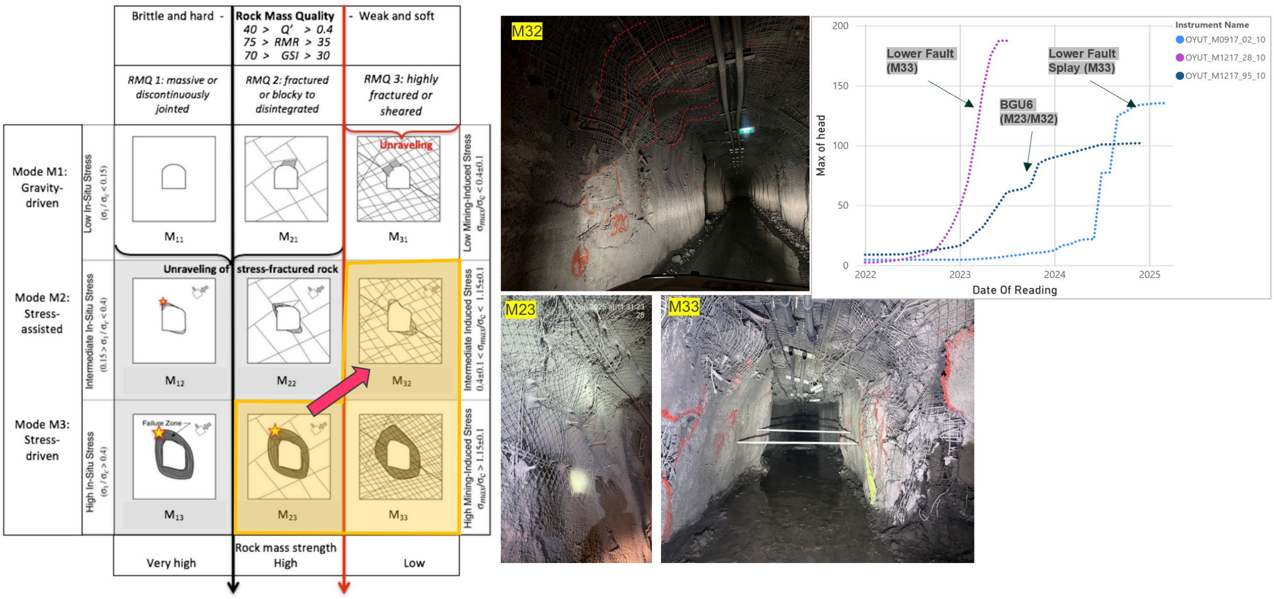

Figure 9 Diagram of dominant damage mechanism at Panel 0 with typical convergence trend plots

4 Numerical analysis

This analysis was undertaken in 3 stages. In the first stage, MPBX and convergence data was prepared for numerical modelling. In the second stage, detailed component scale FLAC3D and PFC3D models assessed damage mechanisms to guide parameter selection for mine scale calibration. In the third stage a mine scale FLAC3D model was calibrated to observed deformation through modification of rock mass strength.

4.1 Preparation of multipoint borehole extensometers and convergence data for numerical modelling

Pre-processed MPBX and convergence data discussed in earlier sections of this paper needs to be prepared for numerical modelling. A 200,000 data points within a 40-month calibration window is required to be spatially and temporally associated with relevant integration nodes. To achieve this task 'numerical instruments' were created at sites using FLAC, combined with multithreaded Java script for numerically expensive computations. It is noteworthy that calibration improved significantly when the model instruments were installed at the same stage as actual instruments. For this reason, when undertaking calibration, clear delineation of total and mining-induced displacement is recommended, as shown in Figure 10.

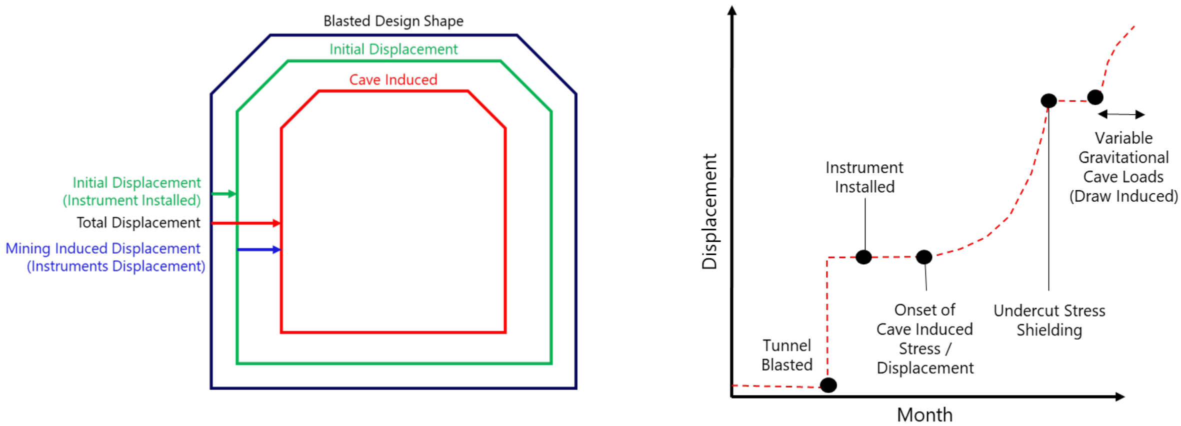

Figure 10 Decomposition of total and mining-induced tunnel convergence

4.2 Conceptual modelling for damage and deformation mechanisms

Detailed mechanistic modelling was undertaken with PFC3D and FLAC3D. In PFC3D, bonded block models (BBM) utilising rigid blocks were embedded at key locations in mine scale FLAC3D models. This approach captured changes in stress and strain resulting from cave geometry and transmitted them to the BBM. For example, the stress path including stress rotation due to undercutting was captured in the BBM.

Model results, combined with observational data were used to formulate damage and deformation mechanisms, and to guide selection of fundamental parameters for the mine scale calibration. One such BBM, for calibrated QMD material, is shown in Figure 11a (domain 6 in Figure 3). It is significant that deformations and damage in this model have good agreement with MPBX and convergence data. The BBM model, as described in Figure 11b, captures the initial formation of the tunnel, historical stress changes, joint activation and shear mobilisation of fractures that exist around the tunnel (Figure 11c).

It is, however, notable that the shape of the excavation damage zone is asymmetric. Likewise, deformation recorded on virtual extensometers is asymmetric, as is the displacement field. This is to be expected in a heterogenous rock mass composed of defects in different orientations (Figure 11d). Heterogenous behaviour also highlights the limitations of models without explicit representation of defects. Conversely, models with defects are strongly dependent on Discrete Fracture Network assumptions.

In consideration of field observations, the dominant damage and deformation mechanisms are:

- shear activation of discontinuities in the excavation sidewalls. This happens some distance from the excavations, outside the zone of excavation damage. The location of defects and orientation relative to mining-induced stress affects the potential for shear activation. Within the stress abutment, stress field 1 (S1) is predominantly vertical, which drives activation of sub-vertical joints and veins located in the excavation sidewalls (Figure 11b).
- formation of stress-driven shear bands and tensile fractures through the rock mass, interacting with discontinuities. Linking of fractures with joints and veins results in the formation of blocks and potential for block rotation (Figure 11c). This can be categorised as Mode 2 and 3 for rock mass quality 2 and 3 materials (Figure 9). Furthermore, the models indicate zones of high stress combined with stress rotation, which induce multiple activated planes of fracturing with different orientations. The undercut front in the last 50% of Hydraulic Radius (HR), in particular, exhibits this behaviour (Figure 3, Domains 5 and 6), while the south abutment does not (Figure 3, domain 1).

4.3 Mine scale model calibration method

The purpose of the mine scale model is to provide a means to assess fundamental aspects of mine scale stability, such as tunnel deformation and pillar stability. The purpose of calibration was to derive material properties matching observed behaviour. It is essential to note that due to the uncertainty and variability of site data, calibrated properties are not unique. As a result, calibrated strength is considered as a range of possibilities to be updated as new information becomes available. The calibration method is described in the following 5 sub-subsections.

4.3.1 Geometry and domain decomposition

Mine geometry and cave shapes are modelled for the temporal window of January 2022 to March 2025 (40 months) at a minimum resolution of one-month time stages.

The footprint was spatially decomposed into 56 calibration domains. These domains emerge from the following spatial decomposition. First, 10 spatial domains were identified as representing different stress paths experienced by excavations (Figures 5 and 12b). Life cycle stress analysis, described later, was used to identify these domains. Within each primary domain are secondary domains defined by geotechnical units (Figure 3a) which are calibration domains.

4.3.2 Statistical modelling of observational data – deformation characteristics curves

Within each calibration domain, data from groups of instruments are reduced to characteristics curves defining a statistical representation of deformation. This representation is the fundamental metric used to calibrate the mine scale model.

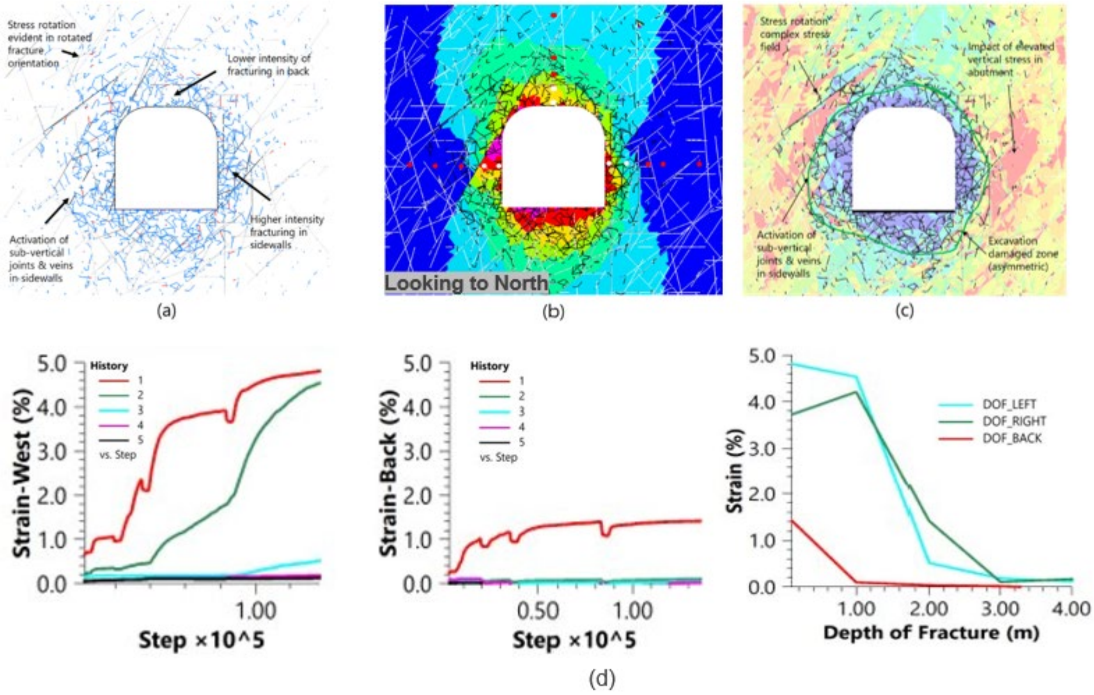

Figure 11 Bonded block model: (a) Deformation mechanisms; (b) Deformation field; (c) S1 stress field; (d) Strain (virtual instruments shown as red dots in the inset b)

4.3.3 Establishment of baseline response

One key finding concerns the importance of establishing a baseline model. This includes careful interpretation of site data and formulation of a model with sufficient granularity to capture observed mechanisms.

A baseline model was constructed using FLAC3D (v9.6.45, ITASCA 2026), adopting:

- A material model: the Hoek–Brown rock mass strength estimation procedure (Hoek & Brown 2019) was utilised in the Itasca Model for Advanced Strain Softening material model (Ghazvinian et al. 2020). Application of the Hoek–Brown procedure was found to be a reasonable starting point for assessing tunnel and pillar deformations. A plot showing the distribution of rock mass uniaxial compressive strength (UCS) is provided in Figure 2b, where the zones of low rock mass strength are indicated in the major fault zones. A limitation of the field data is that major faults were interpreted to have fixed GSI values. By contrast, field data indicates high variability. As a result, discrepancies between modelled and measured deformations emerged in this these zones, resulting in a range of calibrated properties for faults as follows:
- GSI/uniaxial compressive strength of the intact rock (UCSI): GSI was derived from a geotechnical block model while intact rock properties (UCSI, m_i, E_i) were applied within geotechnical units
- Faults: there were 150 explicit faults, with material properties estimated from observed shear displacement corelated to mine seismic data and excavation response
- Cave geometry: shapes were derived from calibrated mechanically coupled FLAC3D-CAVESIM models

- Geometry: mine geometry was sequenced at one month granularity. Excavations were explicitly represented with a support pressure aligned with installed support systems.

4.3.4 Life cycle stress analysis

In addition to conventional plots of stress, tunnel deformation and rock mass plasticity, an algorithm was developed to compute a new parameter called 'life cycle' stress (Figures 12a and b). Life cycle stress is the maximum stress an element of rock experiences during its 'life'. This includes S1 and differential stress. These metrics were conceived to provide a unified visualisation of stress experienced across time in a single plot.

Figures 12a and b show the significant variation in life cycle stress experienced on the extraction level as abutment stress increases due to cave propagation and increase in HR. Life cycle stress strongly correlates with observed deformation (Figures 12c and d). For example, early undercutting prior to significant cave propagation results in relatively low life cycle stress (Figure 12, domain 4). After HR is achieved, cave propagation increases abutment stress (domain 5), resulting in increased deformation. Continued propagation results in further increases in stress (domain 6. Final state abutment stress continues to increase until the cave geometry reaches the final state (domain 1). It is notable that a significant stress partitioning is observed in domain 1 in the final state north abutment due to the presence of a major fault.

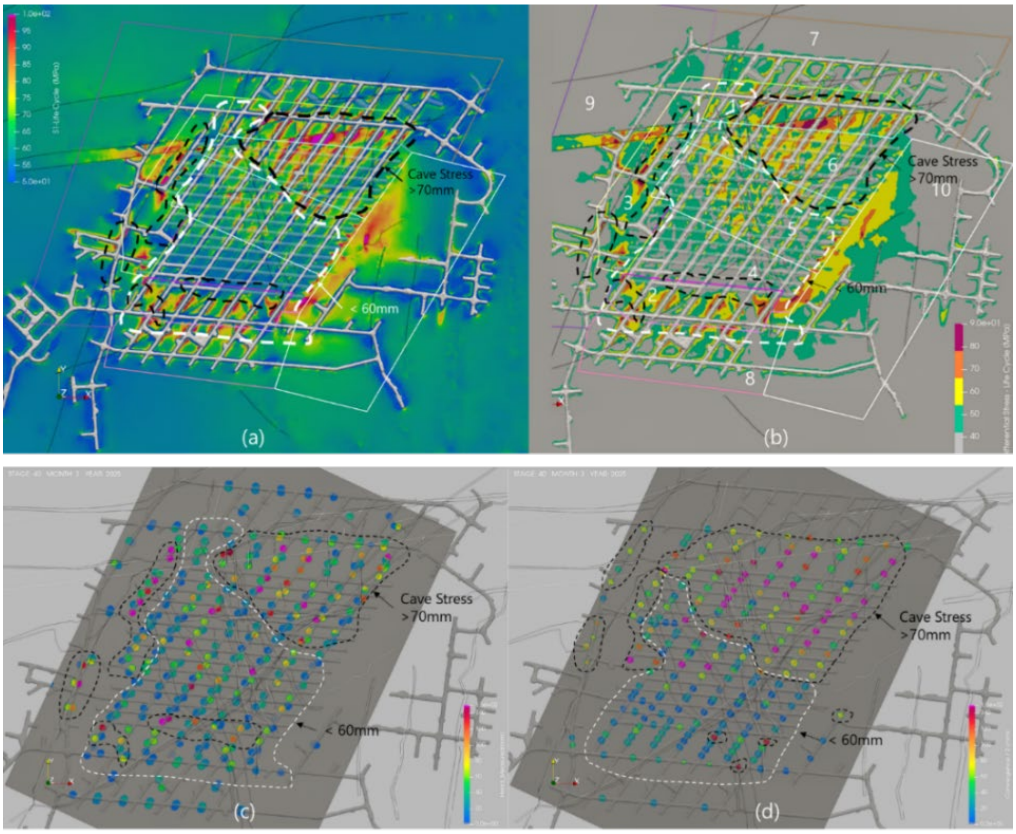

Figure 12 (a) Stress field 1 life cycle; (b) Plastic strain – life cycle; (c) Multipoint borehole extensometers deformation – March 2025; (d) Closurex0.5 – March 2025

4.3.5 Mine scale calibration

Deformation on virtual instruments within each calibration domain was compared against statistical curves for MPBX and convergence data. For each calibration domain a 'characteristics curve' was assembled based on deformation as a function of distance from the undercut abutment (Figure 13). The strength of this method is that calibration considers deformation across a range of stress magnitudes relevant to the primary calibration domain. Even so, data variability is considerable and expected, as shown in Figure 13.

In the calibration stage, rock mass and structural properties in each domain were varied to recover the observed rock mass response. Calibrated strength was expressed as a percentage of the baseline Hoek–Brown strength. For example, for a key lithological unit called QMD, strength in domain 6 to achieve calibration was found to be in the order of 90% baseline. This indicates a reduction of 10% in strength is needed to match observed median deformation.

In addition to matching deformation characteristics curves, an overall comparison of 'model versus measured' damage category was undertaken (Figure 14). It was found that 80% of the measured damage categories were successfully matched using this method. The key source of category mismatch is fault zones (Figure 15. As a result, a range of fault strengths were modelled and further work to delineate GSI variability within faults was recommended (the baseline data assumed constant GSI which FZ1 fault zones).

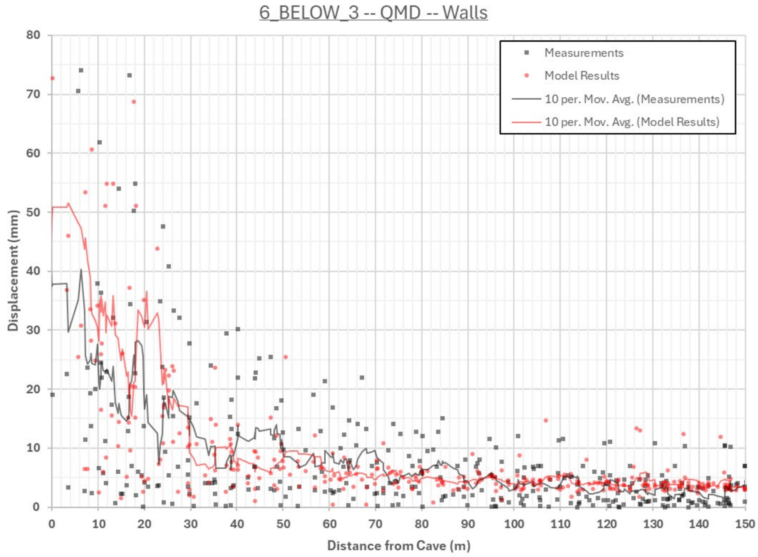

Figure 13 Multipoint borehole extensometer displacement (measured and modelled-calibrated) versus distance from undercut (quartz monzodiorite [QMD]) in the Below_3 area

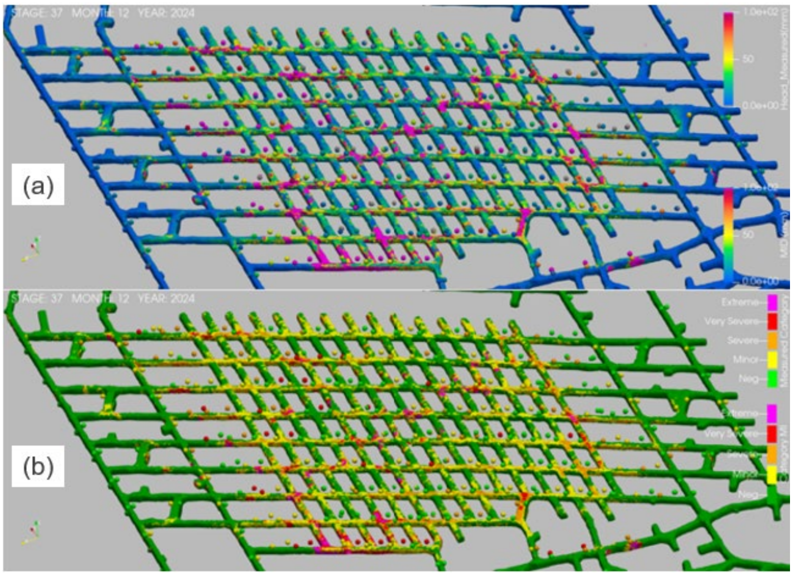

Figure 14 (a) Modelled versus measured displacement and damage category; (b) Categories defined by Marinos & Hoek (2000)

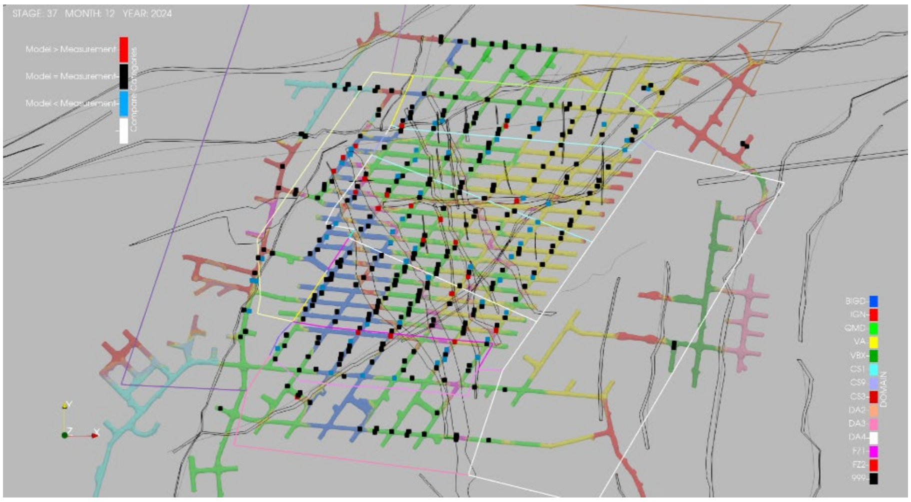

Figure 15 Match between multipoint borehole extensometers measurements and model

4.4 Mine scale and bonded block models interpretation result

Conclusions relating to numerical analysis are described as follows:

- BBMs: these proved useful in building a conceptual model for damage and deformation mechanisms.
- Mine scale calibration method:
  - Decomposition of the model space into calibration domains based on life cycle stress and geotechnical units proved useful.
  - Calibration of clusters of instruments within calibration domains and relative to the undercut stress abutment, and reduction of these data to deformation-distance characteristics, was successful.
  - Installing instruments at the correct times and removing initial displacements improved the model calibration, especially in low-strength materials.
- Baseline properties: for baseline properties, a reasonable match between measured and modelled deformation was achieved outside of FZ1 fault zones. It is concluded that baseline parameters derived using the C method (Hoek & Brown 2019) provided a reasonable fit (within ±15%) to deformation and 'damage category'. This result is useful in guiding the selection of parameters for sensitivity analysis and gives confidence to the applicability of this method in moderate to low-strength rock masses exhibiting shear failure mechanisms.
- Calibrated properties:
  - A good match between measured and modelled deformation was achieved outside of FZ1 fault zones. Model calibration was achieved by reducing strength by 0–15% in some key domains. In these domains a good match between deformation and 'distance from cave' (deformation characteristic curve) was achieved in the high stress abutments (e.g. Domains 5, 6 and 1). Eighty per cent of instrument sites agreed with the measured damage category estimated from MPBX data. Excluding fault zones, most of the damage categories were captured.
  - FZ1 fault strength was found to be variable. In particular, strength was underestimated with the Hoek–Brown (Hoek & Brown 2019) methodology in some locations.

5 Conclusion

This study highlights the critical importance of rigorous data review and quality control prior to interpretation and numerical analysis, particularly in highly instrumented, deep block cave environments. A structured workflow from understanding instrumentation limitations, through QA/QC filtering, to consistent data definition was essential to ensure reliable interpretation of ground response at Panel 0. Grouping monitoring data by both geotechnical domains and stress-change environments proved fundamental in isolating the key drivers of excavation behaviour and reducing the influence of local-scale heterogeneity. This approach enabled meaningful comparison of monitoring datasets and provided a robust basis for interpreting deformation mechanisms under differing stress regimes associated with undercut advance and cave development.

The combined use of mine scale FLAC3D numerical modelling and locally detailed bonded block models successfully replicated observed deformation trends and damage mechanisms, providing strong agreement with measured multipoint borehole extensometers, convergence, and damage mapping data. The selected methodology proved effective for developing a conceptual understanding of ground responses and mechanisms across varying rock mass qualities and stress histories.

Calibration is a continuous iterative process. As mining progresses and new monitoring data become available, repeated calibration is required to progressively refine model confidence and improve forecasting capability. A site investigation of Geological Stability Index variability in future work and testing a range of strengths in forward designs are suggested. This highlights the importance of understanding the location and characteristics of significant fault zones on block cave footprints

Acknowledgement

The authors would like to acknowledge the contributions of the Oyu Tolgoi site geotechnical team for their ongoing commitment to geotechnical monitoring, data collection and technical discussions that made this study possible. The authors also gratefully acknowledge Oyu Tolgoi LLC and Rio Tinto for granting permission to publish this work. In addition, the authors would like to thank Dr Ian Brunton and Dr Karina Barbosa of ITASCA Australia, who assisted with the formulation of the numerical models presented in this paper.

Disclaimer

Please note that this paper contains estimates and forward-looking statements within the meaning of applicable securities laws. These statements are based on assumptions and publicly available or site-observed information available at the time of writing. Actual outcomes may differ due to geotechnical, operational, geological and other factors

References

Bayar, E, Simanjuntak, K, Birch, D, Mardiansyah, F & Purwanto, H 2024, 'Seismological data and analysis for the early stages of block caving', in D Johansson & H Schunnesson (eds), *MassMin 2024: Proceedings of the International Conference & Exhibition on Mass Mining*, Luleå University of Technology, Luleå, pp. 893–908, https://doi.org/10.36487/ACG_repo/2435_G-02

Ghazvinian, E, Garza-Cruz, T, Bouzeran, L, Fuenzalida, M, Cheng, Z, Cancino, C & Pierce, M 2020, 'Theory and implementation of the ITASCA constitutive model for advanced strain softening (IMASS)' in R Castro, F Báez & K, Suzuki (eds), *MassMin 2020: Proceedings of the Eight International Conference & Exhibition on Mass Mining*, Universidad de Chile, Santiago pp. 451–461.

Hoek, E & Brown, ET 2019, 'The Hoek–Brown failure criterion and GSI – 2018 edition', *Journal of Rock Mechanics and Geotechnical Engineering*, vol. 11, no. 3, pp. 445–463.

ITASCA 2026, *FLAC3D (Fast Lagrangian Analysis of Continua)*, version 9.6.45, computer software, ITASCA, Minneapolis.

Laubscher, DH 1990, 'A geomechanics classification system for the rating of rock mass in mine design', *Journal of the South African Institute of Mining and Metallurgy*, vol. 90, no. 10, pp. 257–273.

Marinos, P & Hoek, E 2000, 'Predicting tunnel squeezing problems in weak heterogeneous rock masses', *Tunnels and Tunnelling International*, vol. 32, no. 11.

Ulziijargal, M, Enkhtaivan, E, Purevdorj, M, Purwanto, H, Simanjuntak, K & Moorcroft, T 2024, 'Oyu Tolgoi geotechnical monitoring system', in D Johansson & H Schunnesson (eds), *MassMin 2024: Proceedings of the 9th International Conference & Exhibition on Mass Mining*, Luleå University of Technology, Luleå, pp. 383–397, https://doi.org/10.36487/ACG_repo/2435_C-07